Low-cost air-stable perovskite solar cells by incorporating inorganic materials

Heshmati, N.; Mohammadi, M. R.; Abachi, P.; Martinez-Chapa, S. O.

Published in:
New Journal of Chemistry

DOI:
10.1039/d0nj04619a

Publication date:
2021

Low-cost air-stable perovskite solar cells by incorporating inorganic materials

N. Heshmati[a], M.R. Mohammadi[a,b], P. Abachi[a], S.O. Martinez-Chapa[c]

[a] *Department of Materials Science and Engineering, Sharif University of Technology, Azadi St., Tehran, Iran*

[b] *Tecnologico de Monterrey, Escuela de Ingeniería y Ciencias, Campus Puebla, Vía Atlixcáyotl 2301, Reserva Territorial Atlixcáyotl, CP 72453 Puebla, Pue, Mexico*

[c] *School of Engineering and Sciences, Tecnologico de Monterrey, Ave. Eugenio Garza Sada 2501, Monterrey 64849, NL, Mexico*

Abstract

Herein, we demonstrate a new fabrication strategy for low-cost and stable-operating perovskite solar cells (PSCs) suitable for commercialization. This is performed by fabrication of the device under ambient conditions using $Cs_{0.05}(MA_{0.17}FA_{0.83})_{0.95}\,Pb(Br_{0.17}I_{0.83})_3$ formulation as the mixed cation and halide (MCH) perovskite and $CuInS_2$ (CIS) as the inorganic hole transporting layer. The deposited MCH perovskite with uniform, compact and smooth microstructure containing equiaxed large grains showed excellent thermal and structural stability under intense conditions at 85 °C for 2 h in humid air (i.e., 45% relative humidity). Moreover, it had higher phosphorescence emission, absorption and bandgap energy than the conventional $MAPbI_3$ due to efficient conversion of PbI_2 to the perovskite compound, as further confirmed by XRD analysis. Photovoltaic measurements under operational conditions revealed that MCH-based PSC showed a 27% higher photoconversion efficiency compared with the control device composed of $MAPbI_3$ raised by less charge recombination. CIS-based MCH

device aged for 30 days at 25 °C and 40% humidity retained 91% of the maximum efficiency with low standard deviation of all photovoltaic parameters, indicating excellent potential for industrialization.

Keywords: Solar cells, $CuInS_2$, Mixed cation and halide perovskite, Air-stable.

1. Introduction

During the last decade, organometal halide perovskites have attracted significant attention due to their prominent optoelectronic properties such as direct bandgap, large absorption coefficients and long diffusion length. Solar cell devices based on these perovskites are a pioneer technology in the solar energy conversion field, exhibiting an outstanding power conversion efficiency (PCE) of 22% and 25% in form of tandem devices.[1,2] In their most common version, perovskite solar cells (PSCs) are composed of a layer structure formed on a transparent electrode made of a thin layer of nanoparticulate titania as electron transport layer (ETL), an organometal halide perovskite layer (i.e., $MAPbI_3$ and $FAPbI_3$ as the conventional perovskites), an organic hole transporting layer (HTL) (i.e., Spiro-OMeTAD as the standard one) and a top gold electrode. However, there are concerns related to the degradation of the components upon association with moisture, heat, oxygen, UV light and other potential factors,[3,4] limiting their application in operation. Diverse strategies have been proposed to improve the stability of the components.[5,6,7,8,9] Amending the chemical composition of the perovskite by modifying or combining its anions and cations is an effective mechanism for improving its electronic properties and stability simultaneously.[10,11,12] Due to instability and volatility of the organic components of

$MAPbI_3$ and $FAPbI_3$, their partial or complete replacement by more stable inroganic ones such as Cs has been reported.[13,14,15] The later has an ionic radius of 1.81 Å, which is considerably smaller than that of MA (2.70 Å) or FA (2.79 Å). Not only the inorganic stable $CsPbI_3$ perovskite crystallizes at the high temeparatute of 310 °C, but also its corresponding cell shows lower efficiency than the conventional PSCs.[16,17] In addition, by decreasing the temperature and exposure to ambient air after several minutes, $CsPbI_3$ transforms to the non-perovskite yellow phase.[18] Therefore, the mixed cation perovskite such as $Cs_x(MA_{0.17}FA_{0.83})_{100-x}PbI_3$ has been presented through composition engineering for enhancing the stability of the device by further tuning the bandgap and achieving effective tolerance factor to decrease the **t** value and drive the crystal structure towards a cubic stable phase.[Error! Bookmark not defined.,Error! Bookmark not defined.] Moreover, mixed cation provides a suitable path to reach the bandgap near the infrared range, which enhances the absorption of light.[19,20] The cation size and content control the network symmetry and lead to the change of the optoelectronic properties. For example, higher contents of cesium result in phase segregation and rapid decrease in thermal stability.[3] Therefore, the quantity of cesium is controlled in the range 0.1-0.2 to block the cesium iodide phase development and decrease in trap density, resulting in an increase in PCE.[21] In addition, the partial replacement of FA by Cs gained better moisture stability compared to $FAPbI_3$ perovskite.[22] It is also known that adopting different halides into the perovskite structure gives rise to a shift in the bandgap, the smaller ionic radius of the halogen, the higher bandgap of the perovskite.[23] Moreover, the morphology and microstructure of the perovskite is dependent upon the halide. In the molecular formula $MAPb(I_{1-x}Br_x)_3$ the atomic radius of bromide (1.96 Å) is slightly smaller than that of iodide (2.20 Å); leading

to higher diffusion of Br^- in the solvent and controlling the growth kinetics of perovskite grains. Indeed, PSCs with the highest reported PCEs, using the antisolvent method, have mixed cations and halides composition.[24] In the present work, we follow the same approach using the mixed cation and halide (MCH) $Cs_{0.05}(MA_{0.17}FA_{0.83})_{0.95}\,Pb(Br_{0.17}I_{0.83})_3$ formulation for fabrication of mesoscopic PSCs.

Generally, PSCs with high efficiency were taken utilizing organic materials, such as Spiro-OMeTAD, as HTLs. This material is expensive to synthesize or to acquire, it has a limited conductivity and necessitates the utilization of additives and its stability is questioned.[25,26] For this reason, other possible inorganic HTLs have been recently intensively studied due to their low-cost and higher hole mobility and stability.[27] $CuInS_2$ (CIS) has recently been employed as a promising inorganic HTL due to its suitable bandgap for the solar spectrum, low toxicity and a high extinction coefficient, although the PCEs of their cells are lower than those of Spiro-OMeTAD based devices.[28] Such favorable characteristics of CIS enabled us to construct low-cost and stable PSCs in this work. All cells were fabricated and characterized under ambient conditions of 40% relative humidity to further reduce the device cost and to evaluate their long-term stability.

2. Experimental

2.1. Materials

Fluorine doped tin oxide (FTO) was purchased from Solaronix (Resistance 7 Ω/square). Titanium(IV) tetraisopropoxide (TTIP, 97%), hydrochloric acid (HCl, 37%), N,N-dimethyl formamide (DMF, 99%), dimethyl sulfoxide (DMSO, 99.9%), isopropyl alcohol

(IPA), chlorobenzene (CB, 99.9%), methylammonium (MAI, 99%), formamidinium iodide (FAI, 99%), lead iodide (PbI_2, 99.99%), methylammonium bromide (MABr, 99%), lead (II) bromide ($PbBr_2$, 99.99%) and cesium iodide (CsI, 99.9%) were purchased from Sigma-Aldrich and all of the reagents were used without further purification except CB, which was purified.

2.2. Fabrication of PSCs

FTO substrates were etched with Zn powder and hydrochloric acid, sequentially cleaned with detergent, deionized water, acetone and ethanol in an ultrasonic bath and finally treated under UV-Ozone. A compact sol-gel derived TiO_2 layer as a blocking layer was spin coated on FTO substrates at 2000 rpm for 30 s, followed by annealing at 500 °C for 30 min. TiO_2 sol was prepared by adding a solution of 2.53 mL ethanol containing 35 μL HCl (37% in water) into a mixture of 369 μL TTIP and 2.53 mL ethanol. Subsequently, a mesoscopic TiO_2 with a thickness of ~400 nm was spin coated at 4000 rpm for 20 s using commercial TiO_2 paste diluted in ethanol. The deposited film was dried at 100 °C for 15 min and calcined at 500 °C for 30 min to eliminate the additives from the mesoscopic film. $MAPbI_3$ perovskite film, as a control cell, was deposited by a sequential two-step method. First, 70 μL of 1.5 M PbI_2 solution in a mixed solvent of DMF and DMSO (4: 1) were spun onto the TiO_2 mesoporous film, which was spin coated at 6500 rpm for 5 s, followed by annealing at 70 °C for 30 min. In the second step, the perovskite material was formed on PbI_2-included substrates by spin-coating 200 μL MAI solution (8 mg/mL in IPA) at 4000 rpm for 20 s after 120 s time-loading. $MAPbI_3$ perovskite film was finally annealed at 70 °C for 30 min.

The mixed cation and halide (MCH) perovskite was prepared according to a procedure reported by Saliba et al.[24] Briefly, FAI, PbI_2, MABr and $PbBr_2$ were dissolved in a mixed solvent of DMF and DMSO (4:1). Then CsI, predissolved as a 1.5 M stock solution in DMSO, was added to the mixed perovskite precursor to achieve the desired triple cation composition containing PbI_2 (1.1 M), FAI (1 M), MABr (0.2 M), $PbBr_2$ (0.2 M) and CsI (0.05 M). The perovskite layer was deposited by spin coating in a two steps program at 1000 and 5000 rpm for 10 s and 20 s, respectively. 250 μL of CB as an anti-solvent were injected on the spinning substrate 5 s prior to the end of the program. $Cs_{0.05}(MA_{0.17}FA_{0.83})_{0.95}\,Pb(Br_{0.17}I_{0.83})_3$ perovskite film was finally annealed at 100 °C for 1 h. $CuInS_2$ (CIS) ink (25 mg/mL in chloroform) was deposited on the perovskite film by spin coating at 3000 rpm for 10 s, followed by drying at 100 °C for 10 min. The coating and drying cycles were repeated sevaral times to achieve CIS film as an inorganic HTL with desired thickness. It should be reiterated that all above procedure for device fabrication was carried out under ambient air conditions of 40% relative humidity. Finally, a gold top electrode was thermally evaporated onto the HTL. The detailed process for fabrication of PSCs based on conventional $MAPbI_3$ and mixed cation and halide $Cs_{0.05}(MA_{0.17}FA_{0.83})_{0.95}\,Pb(Br_{0.17}I_{0.83})_3$ perovskites is schematically illustrated in **Figure 1**. $MAPbI_3$ perovskite was prepared by a two-step deposition process, whereas the MCH perovskite formed by a one-step method.

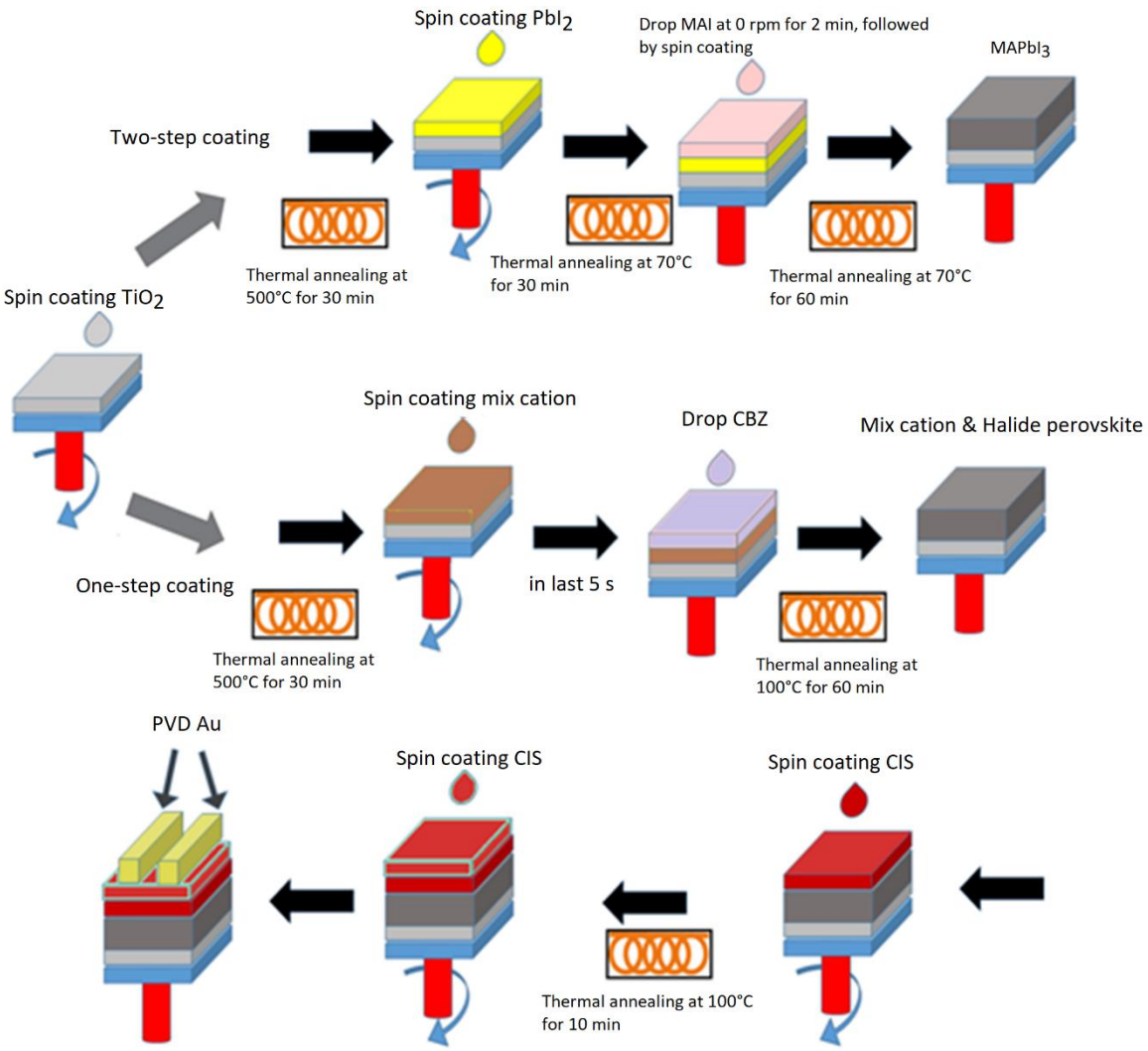

Figure 1. Schematic illustration of the fabrication procedure of PSCs based on conventional and mixed cation and halide perovskites.

2.3. Characterization

Films were characterized in morphology and microstructure using a field emission scanning electron microscope (FESEM) TESCAN−Mira III, in crystal structure and phase composition using an X-ray diffraction (XRD) diffractometer PANalytical X'Pert Pro MPD, Cu Kα radiation (λ = 1.5406 Å) and in optical absorption using an ultraviolet−visible

(UV−vis) absorption spectrum PerkinElmer Lambda 25 spectrophotometer. Steady-state photoluminescence (PL) spectra of the perovskite films were recorded by an AvaSpec 2048 TEC spectrophotometer. Photovoltaic performance of the devices was measured by a solar simulator (SIM-1000 and calibrated by a Thorlabs photodiode) under AM 1.5 (100 mW/cm^2) simulated light radiation, and the active area of the cells was defined to be 0.09 cm^2 using a mask. The current–voltage characteristics were recorded by a Keithley 2400 source meter in reverse scan state from 1.1 V to -0.1 V with the scan rate of 5 mV/s. It should be noted that each batch included five devices and the average values were reported.

3. Results and discussion

We studied optical characteristics and radiative recombination of charge-carriers of the perovskite films by their absorption and photoluminescence (PL) spectra in the visible and ultraviolet regions, as shown in **Figure 2**. The absorption edge of $MAPbI_3$ perovskite was detected around 783 nm, while it was about 777 nm for MCH perovskite (**Figure 2a**), indicating an approximately 6 nm blue shift by introduction of Cs and FA cations and Br halide. Furthermore, a significant increase in absorption of MCH perovskite was attributed to efficient conversion of PbI_2 to the perovskite compound, which is consistent with the results of XRD analysis. Organometal halide perovskites emit substantial photoluminescence, which depends on cation and halide composition.[29] As illustrated in **Figure 2b**, MCH perovskite had higher phosphorescence emission across the 700-800 nm wavelengths than conventional $MAPbI_3$ perovskite, indicating uniform and compact morphology containing large grain size of MCH perovskite and enhanced light absorption

and charge transfer to ETL and HTL films. This is in accordance with high efficiency of PSCs based on mixed cation and halide perovskites.[30,31]

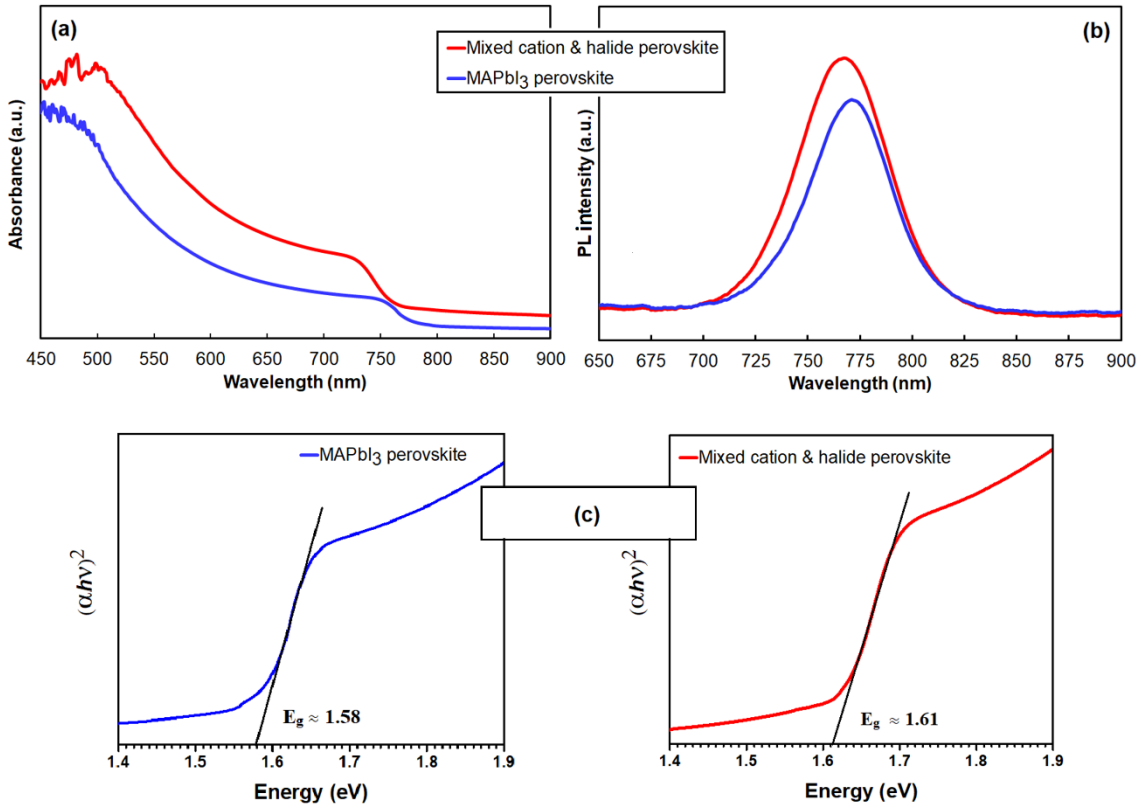

Figure 2. Optical characterisation of the conventional and MCH perovskites: (a) absorption spectra, (b) photoluminescence spectra and (c) optical bandgap calculation.

We detected the emission peak of $MAPbI_3$ perovskite at 770 nm, matched with its direct bandgap raised by recombination of the near band-to-band[32,33] and observed a blue shift by ~5 nm in the PL spectrum of MCH perovskite, which is consistent with that reported previously.[34] The bandgap of perovskites was calculated by linear fits of the absorption edge (Tauc plots), as shown in **Figure 2c**. MCH perovskite showed higher bandgap energy than the conventional $MAPbI_3$ perovskite (1.61 eV vs. 1.58 eV) raised by a reduction in

the effective radius of the A-site cation, resulted in a shrinkage of the network and an increase in the bandgap energy. Although such blue shift may reduce the maximum theoretical photocurrent density of the cell, it is probable to gain higher voltages and suppress charge recombination using materials with larger bandgap absorption.

We further evaluated the thermal stability of the perovskite films under intense condition at 85 °C for 2 h in humid air (i.e., 45% relative humidity), as shown in **Figure 3**. $MAPbI_3$ perovskite presented thermal and structural instability raised by decomposing to PbI_2 as identified by the decreased absorption spectrum, shifted absorption edge from 785 to 520 nm and turned to visibly yellow color. Interestingly, superior thermal and structural stability was achieved for the MCH perovskite with comparatively stable absorption edge and spectrum, retaining the dark black color.

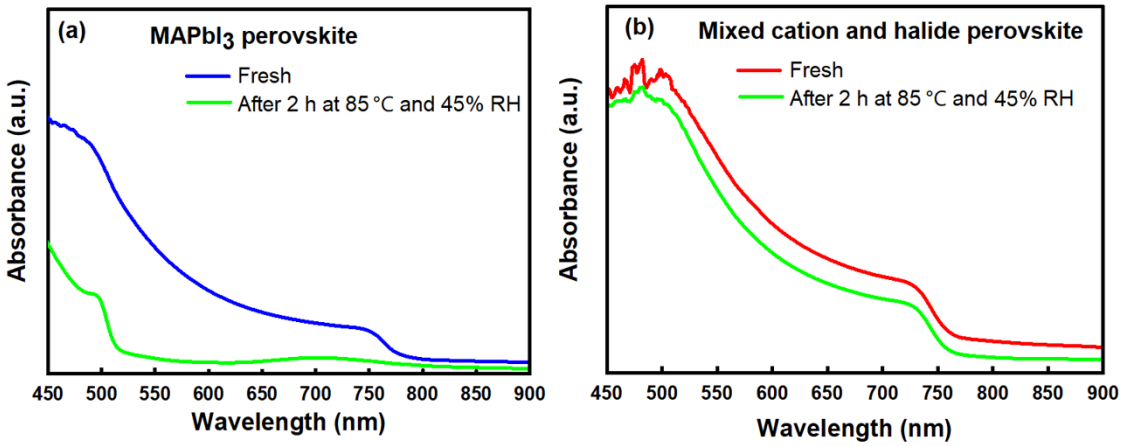

Figure 3. Comparison the thermal and structural stability of perovskite films under intense condition at 85 °C for 2 h in humid air (i.e.,45% relative humidity): (a) $MAPbI_3$ and (b) and MCH perovskites.

Figure 4 shows X-ray diffraction (XRD) data of deposited $MAPbI_3$ and MCH perovskites on FTO/TiO_2 substrate. Both compounds exhibited a typical tetragonal perovskite crystal structure with the strongest peak at 2θ = 14.1° corresponding to (1 1 0) plane. The peaks detected at 2θ = 26.5° and 37.8° are assigned to mesoporous TiO_2 and FTO substrate, respectively. For $MAPbI_3$ (**Figure 4a**), we observed an incomplete conversion of yellow phase perovskite to the photoactive black cubic phase due to presence of PbI_2 peak detected at 2θ = 12.7°, resulted in a reduction in photovoltaic performance of the cell. Upon addition of CS and FA cations and Br halide (**Figure 4b**), not only the yellow phase and the PbI_2 peak disappeared completely, but also the crystallinity and orientation of the perovskite were enhanced.

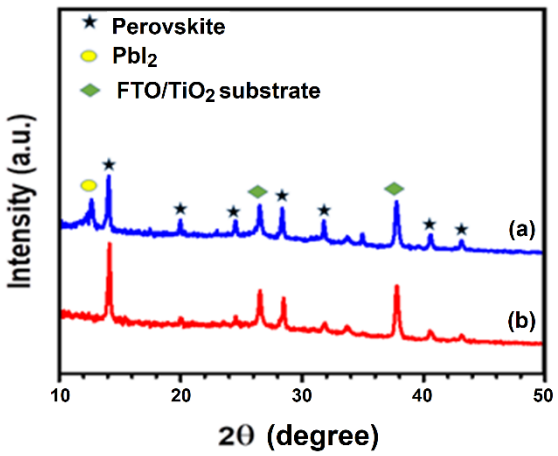

Figure 4. X-ray diffraction (XRD) patterns of: (a) $MAPbI_3$ and (b) MCH perovskites deposited on FTO/TiO_2 substrate.

In **Figure 5**, we show top view FESEM images of the subsequent layers making PSC devices, including compact TiO_2, mesoporous TiO_2, $MAPbI_3$ and MCH perovskites. Both compact- and meso-TiO_2 films (**Figures 5a and 5b**) have highly homogeneous

morphology containing nanometric spherical particles, being in the range 20-25 nm for the meso-TiO_2. It is clear that the size of the perovskite particles is remarkably affected by the incorporation of CS, FA cations and Br halide in the perovskite precursors. The average grain size of $MAPbI_3$ perovskite is in the range of 500-700 nm, whereas it is in the range of 1000-1200 nm for MCH perovskite (**Figures 5c and 5d**). The inset of Figure 5d shows EDS mapping of Cs, indicating uniform distribution of cesium within MCH perovskite.

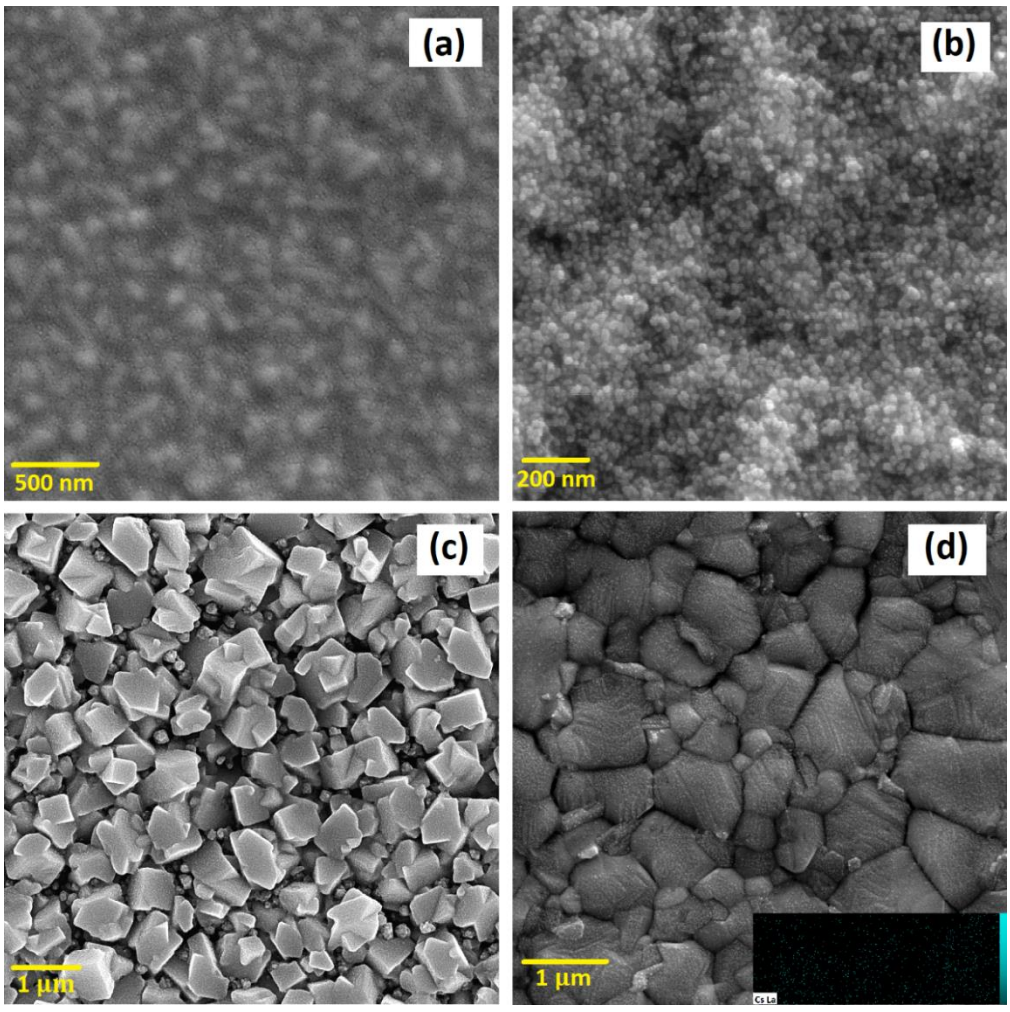

Figure 5. FESEM top views of the subsequent layers making PSC devices: (a) compact TiO_2, (b) mesoporous TiO_2, (c) $MAPbI_3$ perovskite and (d) $\mathbf{Cs_{0.05}(MA_{0.17}FA_{0.83})_{0.95}\ Pb(Br_{0.17}I_{0.83})_3}$ perovskite, the inset shows EDS mapping of Cs.

The larger grain size is expected to increase the charge output efficiency and suppress the recombination at the grain boundaries. Moreover, we can observe that the introduction of CS and FA cations and Br halide leads to the improvement of the perovskite morphology with more uniform, compact and smooth microstructure, compared to the conventional $MAPbI_3$ perovskite. Such a continuous, flat and full coverage MCH perovskite with larger crystals can guarantee the PSC device functioning by preventing a direct contact between ETL and HTL. Therefore, the mixed cation and halide formulation has a positive impact not only on tailoring the perovskite film morphology, but also on converting the residual PbI_2 into perovskite material.

The current density–voltage (J–V) curves and photovoltaic characteristics (i.e., open circuit voltage, short circuit current, fill factor and PCE) of fresh PSCs composed of $MAPbI_3$ perovskite (as the control cell) and MCH perovskite are illustrated in **Figure 6.** It should be reiterated that all devices were constructed under ambient conditions of 40% relative humidity. $MAPbI_3$-based PSC, as the control device, exhibits J_{SC} of 21.30 mA/cm^2, V_{OC} of 0.89 V and FF of 0.447, resulting in an overall PCE of 8.47%. The incorporation of Cs and FA cations and Br halide improved the photovoltaic characteristics of the PSC device. This result is in agreement with those reported in the literature,[24] where a mixed cation and halide in the perovskite composition improved cell efficiency, thanks to greater diffusion coefficients, diffusion lengths and lifetimes of electron–hole pairs in the MCH perovskite absorbers. In addition, the FESEM graphs depict that the grain size of the perovskite film was remarkably increased by the incorporation of the mixed cation and halide within the perovskite precursors. The less the grain boundary content, the higher the

diffusion length. In addition, all fabricated devices showed good reproducibility due to low experimental error of the photovoltaic parameters (inset of Figure 6-b).

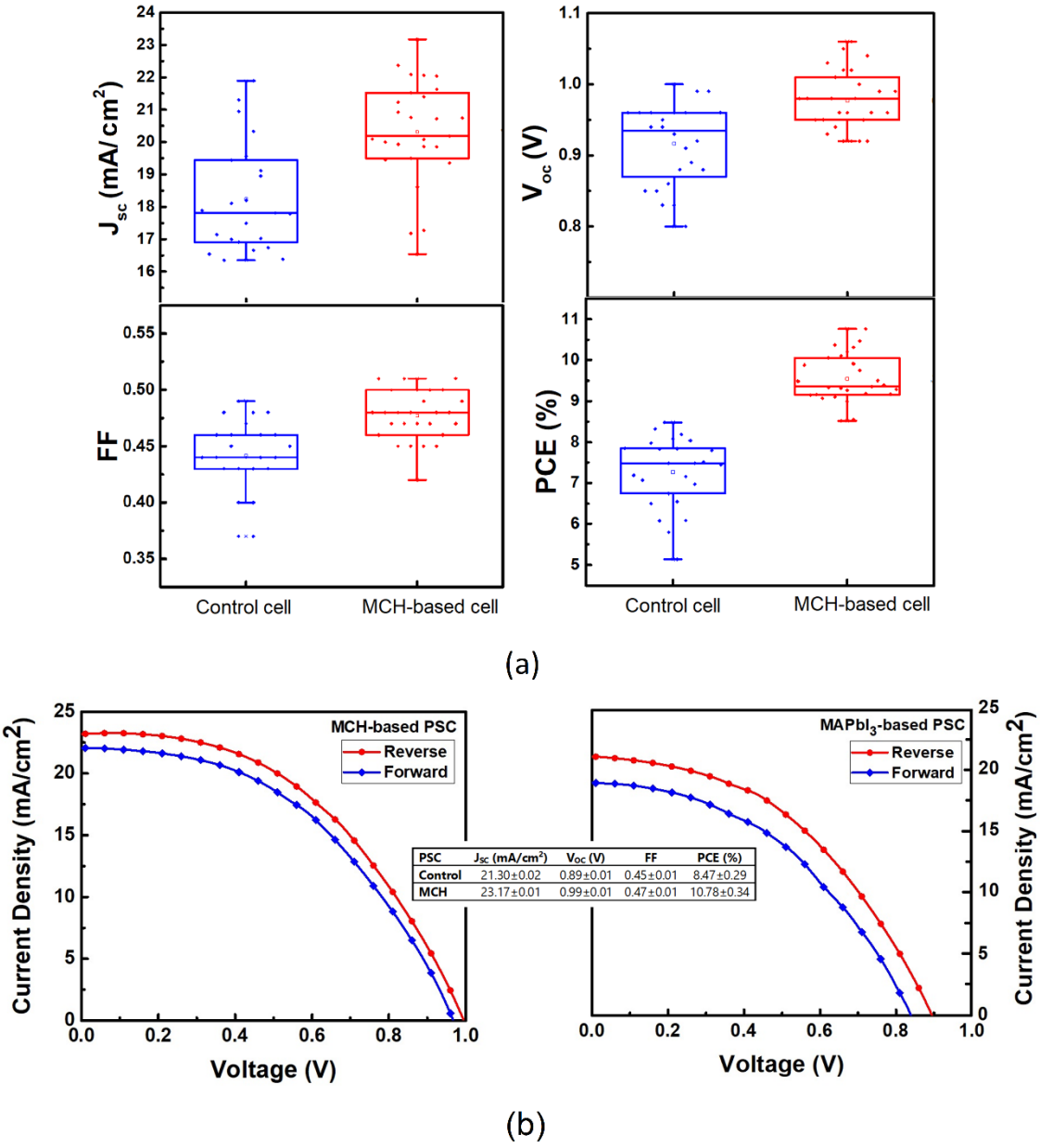

Figure 6. Photovoltaic characteristics of PSC devices made by the conventional $MAPbI_3$ (as the control cell) and $\mathbf{Cs_{0.05}(MA_{0.17}FA_{0.83})_{0.95}\ Pb(Br_{0.17}I_{0.83})_3}$ perovskites: (a) box plot of photovoltaic parameters and (b) current–voltage curves of the champion devices.

Therefore, MCH-based cell with J_{SC} of 23.17 mA/cm^2 and V_{OC} of 0.99 V showed a 27% higher photoconversion efficiency (i.e., PCE of 10.78%) compared with the $MAPbI_3$-based device. Such enhancement in V_{OC} and J_{SC} can be assigned to the higher light absorption (see **Figure 2a**), formation of a uniform and smooth polycrystalline film with equiaxed large grains with reduced traps (see **Figure 5d**) and converting the residual PbI_2 into a perovskite material (see **Figure 4**). Since the devices were constructed under ambient air conditions using an inorganic HTL (i.e., CIS), the highest achieved PCE in the present work is lower than those of cells fabricated in the glove box using standard HTL (i.e., Spiro-OMeTAD) with a PCE beyond 22%. The main impact of CIS can be seen in FF drop of the cells.

We studied long-term stability of high performance $MAPbI_3$- and MCH-based devices in air atmosphere held at room temperature and 40% humidity, as shown in **Figure 7**. A J-V scan was recorded periodically up to 30 days to extract the observed photovoltaic parameters of the champion devices. It is evident that all photovoltaic characteristics of the control device made of $MAPbI_3$ perovskite undergo a rapid deterioration after 15 days of cell operation, while the MCH-based device is much more stable up to 30 days. Intense drop of J_{SC} for the control cell can be related to low light absorption raised by α to δ phase transformation of the perovskite absorber. The more δ phase content, the more recombination and reduction in FF and PCE. Therefore, the fresh $MAPbI_3$-based device presented the highest performance of 8.74% with rapid drop of efficiency in 7 days and 96% loss in 30 days. For MCH-based device, its efficiency demonstrated an increase of

about 1% in the first 3 days, reaching to 11.55% (**Figure 7e**) and then it was followed by some loss of efficiency, finally stabilizing at about 10.52%.

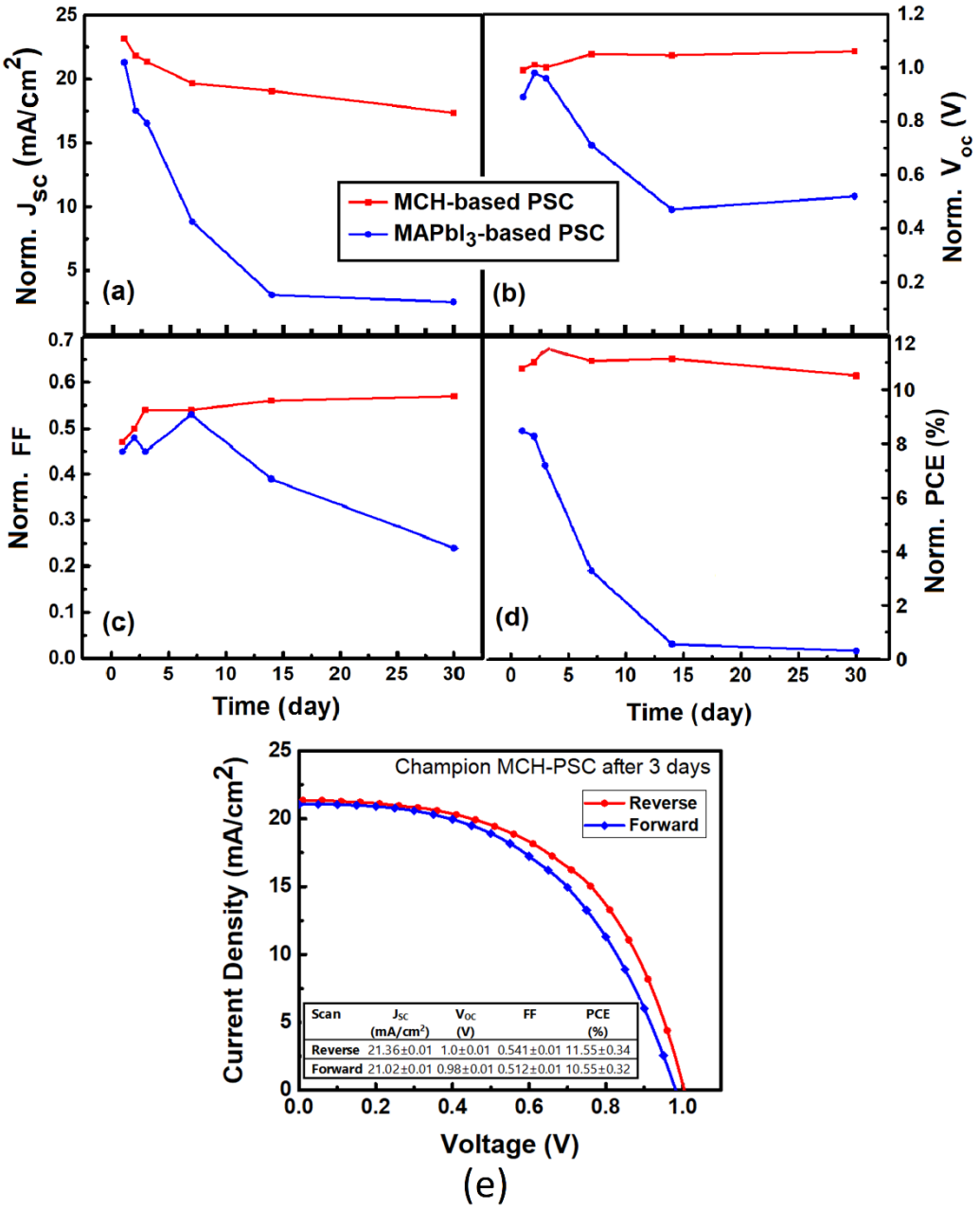

Figure 7. Stability of $MAPbI_3$- and MCH-based PSCs under ambient conditions with 40% RH by comparing their normalized photovoltaic metrics: (a) J_{SC}, (b) V_{OC}, (c) FF, (d) PCE and (e) current–voltage curve of champion MCH-based cell after 3 days.

Such remarkable stability of MCH-based PSC can be attributed to the stability of the α phase and the uniform, compact and smooth microstructure with large grains of the perovskite layer. This implies that introduction of Cs and FA cations and Br halide can significantly enhance the cubic phase stability and delay the degradation of the perovskite, retaining about 91% of the maximum device efficiency. The addition of Br^- promotes charge transfer performance by bandgap tuning. Furthermore, the coexistence of Cs^+ and Br^- not only leads to an increase in grain size of the perovskite, but also induces a contraction of perovskite crystal structure, enhancing its moisture resistance.[35,36]

Figure 8 shows the statistics of MCH-based PSCs by aging for 30 days under ambient temperature (~25 °C) and humidity (40%). We observe almost low standard deviation of all photovoltaic parameters, verifying good potential of CIS-based HTL device for the reproducibility. Therefore, the presented method will open a new concept for up-scaling low-cost efficient and stable PSC devices.

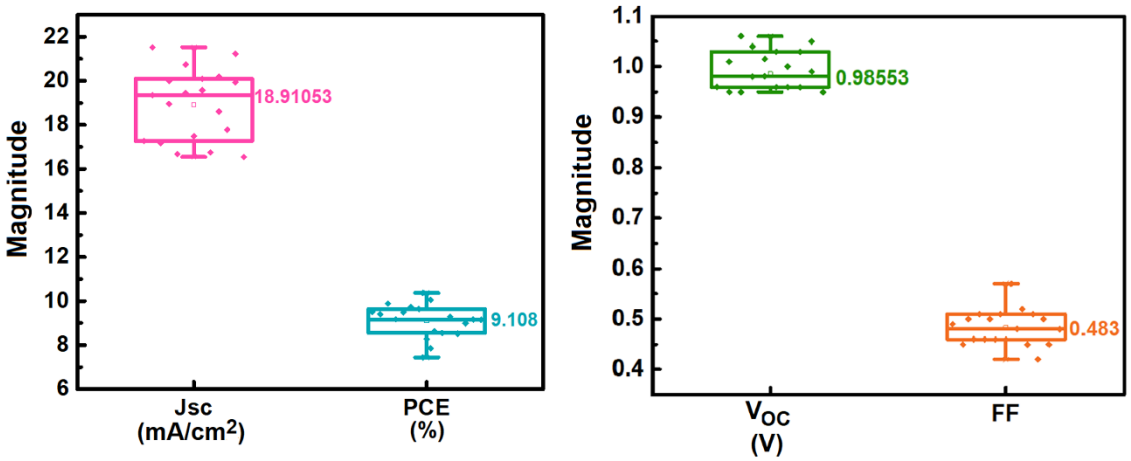

Figure 8. Statistics of fabricated MCH-based PSCs under ambient conditions and aged for 30 days in air atmosphere held at room temperature and 40% relative humidity.

4. Conclusions

In summary, we report a facile method for construction of stable PSC device under ambient conditions using the mixed $Cs_{0.05}(MA_{0.17}FA_{0.83})_{0.95}\ Pb(Br_{0.17}I_{0.83})_3$formulation and the inorganic HTL made of $CuInS_2$. The impact of Cs and FA cations and Br halide incorporation into conventional $MAPbI_3$ perovskite on its physical, optical and photovoltaic characteristics is studied. Thermal and operational stability of CIS-based MCH device are also investigated under intense (i.e., at 85 °C and 45% humidity) and ambient (i.e., 25 °C and 40% humidity) conditions, respectively. Adding the mixed cations and halide suppresses yellow phase impurities and induces highly crystalline uniform and compact perovskite film with large grains which reduce charge recombination. Furthermore, an increase in absorption and bandgap energy of MCH perovskite with a blue shift in the PL and absorption spectra are observed raised by a reduction in the effective radius of the A-site cation and a shrinkage of the crystal structure. MCH device based on inorganic CIS HTL show superior thermal and operational stability up to 30 days, retaining about 91% of the maximum device efficiency with low standard deviation of the photovoltaic parameters. This indicates that there still is enormous potential in development of the presented method using $CuInS_2$ as an encouraging HTL for up-scaling and industrialisation of PSC devices.

References

1 M. Grätzel, *Acc. Chem. Res.*, 2017, **50**, 487-491

2 T. Todorov, O. Gunawan and S. Guha, *Mol. Syst. Des. Eng.*, 2016, **1**, 370-376.

3 G. Niu, W. Li, J. Li, X. Liang, and L. Wang, *RSC Adv.*, 2017, **7**, 17473–17479.

4 G.G. Guzmán, C.F. Peña Camargo, L.C. Luis Rincón, *J. Alloys Compounds*, 2018, **750**, 286–291.

5 B. Salhi, Y. S. Wudil, M. K. Hossain, A. Al-Ahmed, and F. A. Al-Sulaiman, *Renew. Sustain. Energy Rev.*, 2018, **90**, 210–222.

6 K. Qin, B. Dong, and S. Wang, *J. Energy Chem.*, 2019, **33**, 90–99.

7 F. Bella, *Electrochimica Acta*, 2015, **175**, 151-161.

8 A. Abate, J.P. Correa-Baena, M. Saliba, M.S. Su'ait and F. Bella, *Chem. Eur. J.***,** 2018, **24**, 3083-3100.

9 L. Fagiolari and F. Bella, *Energy Environ. Sci.*, 2019, **12**, 3437-3472.

10 H. F. Zarick, N. Soetan, W. R. Erwin, and R. Bardhan, *J. Mater. Chem. A*, 2018, **6**, 5507–5537.

11 M. Datt Bhatt and J. Sung Lee, *New J. Chem.*, 2017, **41**, 10508-10527.

12 R. Azmi, S. Hwang, W. Yin, T.W. Kim, T. Kyu Ahn and S.Y. Jang, *ACS Energy Letters*, 2018, **3**, 1241-1246**.**

13 Y. Hyun Song, S. Hee Choi, W. Kyu Park, J. Sun Yoo, B. Kyun Kang, S. Bin Kwon, H. Suk Jung, W. Seok Yang and D. Ho Yoon, *New J. Chem.*, 2017, **41**, 14076-14079.

14 F. Bella, P. Renzi, C. Cavallo, and C. Gerbaldi, *Chem. A Eur. J.*, 2018, **24**, 12183–12205.

15 F. Xu, T. Zhang, G. Li, and Y. Zhao, *J. Mater. Chem. A*, 2017, **5**, 11450–11461.

16 M. Aamir, T. Adhikari, M. Sher, N. Revaprasadu, W. Khalid, J. Akhtar and J. M. Nunzi, *New J. Chem.*, 2018, **42**, 14104-14110.

17 C. Fai Jonathan Lau, Z. Wang, N. Sakai, J. Zheng, C. Haw Liao, M. Green, S. Huang, H. J. Snaith, A. Ho-Baillie, *Adv. Energy Mater.*, 2016, **9**, 1901685.

18 G. E. Eperon, G. M. Paternò, R. J. Sutton, A. Zampetti, A. A. Haghighirad, F. Cacialli and H. J. Snaith, *J. Mater. Chem. A*, 2015, **3**, 19688–19695.

19 R. Ganesan, S. P. Vinodhini, V. Balasubramani, G. Parthipan, T. M. Sridhar, R. Arulmozhi and R. Muralidharan, *New J. Chem.*, 2019, **43**, 15258-15266.

20 D. Liu, H. Jing, R. Sa and K. Wu, *New J. Chem.*, 2019, **43**, 9453-9457.

21 Y. Wu, W. Chen, G. Chen, L. Liu, Z. He, and R. Liu, *Nanomaterials*, 2018, **8**, 1–27.

22 J. W. Lee, D. H. Kim, H. S. Kim, S. W. Seo, S. M. Cho, and N. G. Park, *Adv. Energy Mater.*, 2015, **5**, 1501310.

23 Y. Liu, Z. Yang, D. Cui, X. Ren, J. Sun, X. Liu, J. Zhang, Q. Wei, H. Fan, F. Yu, X. Zhang, C. Zhao, S. (Frank) Liu, *Adv. Mater.*, 2015, **27**, 5176–5183.

24 M. Saliba, T. Matsui, Ji-Youn Seo, K. Domanski, Juan-Pablo Correa-Baena, M. Khaja Nazeeruddin, S. M. Zakeeruddin, W. Tress, A. Abate, A. Hagfeldt and M. Gratzel, *Energy Environ. Sci.*, 2016, **9**, 1989-1997.

25 E. Nouri, Y.L. Wang, Q. Chen, J.J. Xu, G. Paterakis, V. Dracopoulos, Z.X. Xu, D. Tasis, M.R. Mohammadi and P. Lianos, *Electrochimica Acta*, 2017, **233**, 36–43.

26 T.N. Huan, D.A. Dalla Corte, S. Lamaison, D. Karapinar, L. Lutz, N. Menguy, M. Foldyna, S.H. Turren-Cruz, A. Hagfeldt, F. Bella, M. Fontecave and V. Mougel, *Proceedings of the National Academy of Sciences*, 2019, **116**, 9735-9740.

27 R. Singh, P. K. Singh, B. Bhattacharya and H.W. Rhee, *Applied Materials Today*, 2019, **14**, 175-200.

28 Y. Liu, Z. Zhang, H. Gao, H. Zhang, and Y. Mao, *Org. Electron.*, 2019, **75**, 105430.

29 B.R. Sutherland and E.H. Sargent, *Nature Photonics*, 2016, **10**, 295–302.

30 Y. Kanemitsu, *J. Mater. Chem. C*, 2017, **5**, 3427–3437.

31 L. Gouda, R. Gottesman, S. Tirosh, E. Haltzi, J. Hu, A. Ginsburg, D. A. Keller, Y. Bouhadana and A. Zaban, *Nanoscale*, 2016, **8**, 6386–6392.

32 C. Roldán-Carmona, P. Gratia, I. Zimmermann, G. Grancini, P. Gao, M. Graetzel and M. Khaja Nazeeruddin, *Energy Environ. Sci.*, 2015, **8**, 3550–3556.

33 F. Jiang, Y. Rong, H. Liu, T. Liu, L. Mao, W. Meng, F. Qin, Y. Jiang, B. Luo, S. Xiong, J. Tong, Y. Liu, Z. Li, H. Han, Y. Zhou, *Adv. Funct. Mater.*, 2016, **26**, 8119–8127.

34 C. Yi, J. Luo, S. Meloni, A. Boziki, N. Ashari-Astani, C. Grätzel, Shaik M. Zakeeruddin, U. Röthlisberger and M. Grätzel, *Energy Environ. Sci.*, 2016, **9**, 656–662.

35 Z. Li, M. Yang, J. S. Park, S. H. Wei, J. J. Berry, and K. Zhu, *Chem. Mater.*, 2016, **28**, 284–292.

36 S. Lv, S. Pang, Y. Zhou, N. P. Padture, H. Hu, L. Wang, X. Zhou, H. Zhu, L. Zhang, C. Huang, G. Cui, *Phys. Chem. Chem. Phys.*, 2014, **16**, 19206–19211.